Synthesis and Properties of AB-Type Semicrystalline Polyimides Prepared from Polyamic Acid Ethyl Ester Precursors

Xiang-Qian Liu, Mitsutoshi Jikei, and Masa-aki Kakimoto*

Department of Organic and Polymeric Materials, Tokyo Institute of Technology, 2-12-1, O-okayama, Meguro-ku, Tokyo, 152-8552 Japan

Received October 30, 2000; Revised Manuscript Received February 20, 2001

ABSTRACT: Three AB-type polyimides with para-, meta- and ortho-linked main chain units based on hydroquinone, resorcinol and catechol, were synthesized and characterized. The polyimides were prepared in two steps by the direct polycondensation reactions of isomeric monomers, 4-(4-aminophenoxy)diphenyl ether-3′,4′-dicarboxylic acid monoethyl ester (I_p), 3-(4-aminophenoxy)diphenyl ether-3′,4′-dicarboxylic acid monoethyl ester (I_m) and 2-(4-aminophenoxy)diphenyl ether-3′,4′-dicarboxylic acid monoethyl ester (I_o), to form poly(amic acid ethyl ester)s followed by thermal or chemical imidization. The resultant polyimides were analyzed by tensile tests, thermogravimetry (TG), differential scanning calorimetry (DSC), dynamic mechanical analysis (DMA), and wide-angle X-ray diffraction measurements. It was shown that these AB-type polyimides were semicrystalline and the crystallinities were estimated to be 19−24%. These polyimides showed glass transition temperatures in the range of 178−198 °C and melting transition temperatures of 308−393 °C. DSC measurements suggested that the polyimide based on hydroquinone units crystallizes much faster than those based on resorcinol and catechol. The polyimide based on the fully para-ether linkages showed a single melting endotherm, whereas the polyimides containing meta- and ortho-ether linkages exhibited bimodal melting behavior.

Introduction

Aromatic polyimides are one of the most important high-performance polymers. Because of their excellent electrical, thermal, and high-temperature mechanical properties, aromatic polyimides have found many applications in advanced technologies.[1,2] Semicrystalline polyimides provide the further advantages of enhanced resistance to organic solvents and bases, retention of mechanical properties above their glass transition temperature, and high thermooxidative stability. Many attempts have focused on semicrystalline aromatic polyimides over recent years.[3−12] Melt processing is more desirable both in terms of cost and environmental friendliness; thus, the synthesis of thermoplastic and thermally stable aromatic polyimides is of prime interest. The efficient approaches to lower the glass transition temperature and melting transition temperature have involved the addition of flexible ether and carbonyl linkages, as well as the introduction of meta-substituted aromatic rings.[13−17]

All commercial thermoplastic aromatic polyimides are produced from the AA/BB monomer systems. To our knowledge, there is currently no thermoplastic aromatic polyimide prepared from direct polycondensation of AB-type monomers. From a practical point of view, using AB-type monomer to prepare thermoplastic aromatic polyimides can provide further advantages in the preparation and processing of this kind of materials, since the ratio of two functional groups, "A" and "B", is limited to 1:1. Therefore, the AB-type monomer provides the possibility to be thermally polymerized and processed whereas the traditional AA−BB type polyimides cannot be thermally polymerized and most of them cannot be thermally processed. Recently, we have studied the direct polycondensation of an AB-type isomeric mixture of *m*- and *p*-monomethyl 4-(4′-aminophenoxy)phthalate.[18] Via a two-step method, semicrystalline poly[4-(4′-phenoxy)phthalimide] was successfully prepared with a glass transition temperature of 260 °C, melting transition temperature of 528 °C, 10% weight loss temperature of 575 °C, and crystallinity of 20−31%. Unfortunately, it was difficult to melt process since the melting transition temperature is close to the decomposition temperature.

On the basis of these results, three novel AB-type isomeric mixtures, 4-(4-aminophenoxy)diphenyl ether-3′,4′-dicarboxylic acid monoethyl ester (I_p), 3-(4-aminophenoxy)diphenyl ether-3′,4′-dicarboxylic acid monoethyl ester (I_m) and 2-(4-aminophenoxy)diphenyl ether-3′,4′-dicarboxylic acid monoethyl ester (I_o) were synthesized from 4-nitrophthalonitrile and hydroqinone, resocinol and catechol, respectively. The direct polycondensation and subsequent imidization, as well as thermal and mechanical properties of the resulting polyimides, were also investigated in this paper. The bimodal melting behavior, which was observed for AB-type semicrystalline aromatic polyimides based on resorcinol and catechol, was also discussed.

Results and Discussion

Synthesis and Characterization. The isomeric AB-type monomers I_p, I_m, and I_o were successfully synthesized by hydrogenation of their corresponding nitro substituted compounds, which were prepared from the ring-opening reaction of the respective anhydrides with ethanol, as shown in Scheme 1. The structure of these monomers as well as the intermediates was confirmed by elemental analysis, infrared spectra (IR), and ^{1}H NMR spectra. Figure 1 shows the ^{1}H NMR spectra of monomer I_p, I_m, and I_o along with their assignments. The isomer ratios of these monomers calculated from the integration of the proton peaks meta to the ether linkage (g peaks in Figure 1) were 70/30 (I_p), 68/32 (I_m), and 72/28 (I_o) for *m*-/*p*-ethyl ester isomer.

* Correspondence author. Telephone: +81-3-5734-2433. Fax: +81-3-5734-2875. E-mail: mkakimot@o.cc.titech.ac.jp.

10.1021/ma001862n CCC: $20.00
Published on Web 04/05/2001

Scheme 1

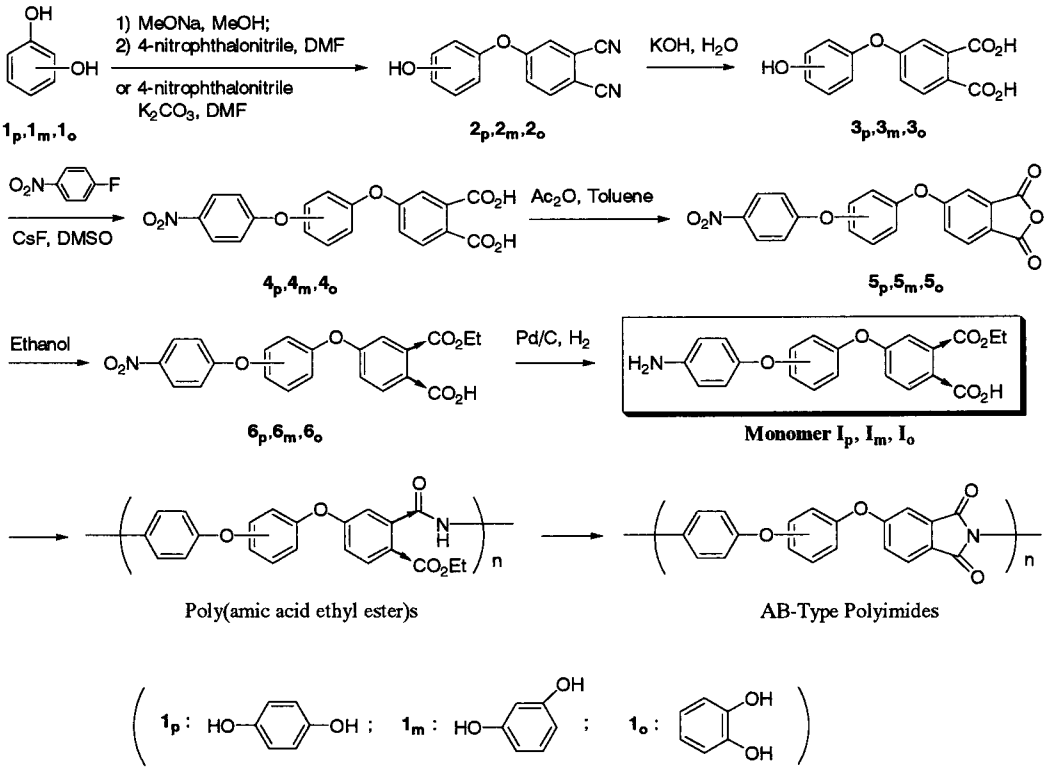

The AB-type polyimides were prepared by a two-step method as shown in Scheme 1. Direct polycondensation reactions of monomer I_p, I_m, and I_o were carried out in the presence of diphenyl(2,3-dihydro-2-thioxo-3-benzoxazolyl)phosphonate (DBOP) and triethylamine. The results are presented in Table 1. The poly(amic acid ethyl esters)s $PAEE_p$, $PAEE_m$, and $PAEE_o$ with relatively high molecular weights ($M_n > 3.5 \times 10^4$) can be readily obtained in good yields under the polymerization conditions used, indicative of the sufficient purity of these AB-type monomers without further purification. The PAEEs exhibited good solubility in organic solvents, such as acetone, THF, DMF, DMSO, DMAc, and NMP.

The PAEEs obtained were characterized by IR and ^{1}H NMR spectra. The characteristic absorptions of amide groups were clearly observed at 1670 cm^{-1} in the IR spectra of $PAEE_p$, $PAEE_m$, and $PAEE_o$, and the specific resonance at ca. 10.3 ppm in the ^{1}H NMR spectra of these precursors also supported the structures of PAEEs.

The thermal behaviors of these PAEEs were investigated by TG/DTA and DSC measurements. All the TG curves of $PAEE_p$, $PAEE_m$, and $PAEE_o$ exhibited two-step drops at ca. 200 and 560 °C. The first and the second weight losses were associated with the elimination of ethanol generated by imidization and with the decomposition of resulting polyimides, respectively. The three precursors displayed similar thermal behaviors. From DSC measurements of these precursors (as shown in Figure 2), the glass transition temperatures were observed, as well as a large endotherm related to the thermal imidization process in all cases. The glass transition temperatures were observed at 158 °C for $PAEE_p$, 141 °C for $PAEE_m$, and 147 °C for $PAEE_o$. These results suggested that the segmental mobility has an order of $PAEE_m > PAEE_o > PAEE_p$. It should be noted that the peak value of the endotherm due to imidization increased in the order of $PAEE_p$ (202.5 °C), $PAEE_m$ (209.7 °C), and $PAEE_o$ (214.6 °C), probably implying that the structure of $PAEE_p$ is more favorable for imidization than that of $PAEE_m$ and $PAEE_o$. For $PAEE_p$, a large exotherm related to the crystallization of the resulting polyimide was observed after the imidization endotherm. Finally, a clear endotherm related to the melting transition of the polyimide crystals can be observed. However, neither exotherm nor endotherm was observed after imidization of $PAEE_m$ and $PAEE_o$. These results indicate that the polyimide based on hydroquinone is easy to crystallize during the thermal imidization of the precursor $PAEE_p$, even at a heating rate of 10 °C/min. On the other hand, the resulting polyimides cannot be crystallized under the same condition when the middle para-substituted benzene in repeating unit was changed to meta or ortho substitutions.

Three precursors were converted to the corresponding polyimides using both chemical and thermal methods. During the chemical imidization, precipitation was observed for the case of $PAEE_p$ and $PAEE_m$. To complete the imidization, all polyimides were dried in a vacuum at 250 °C overnight and at 300 °C for 1 h after isolation from the chemical imidization process.[11]

The structure of the resulting polyimides was characterized by means of IR spectroscopy. IR spectra confirmed the completion of imidization process both in thermal and chemical cyclodehydration. The characteristic absorption bands of the amide groups at around 3370 and 1667 cm^{-1} disappeared, and those of the imide groups were clearly observed at 1778 (asym C═O str), 1720 (sym C═O str), 1390 (C−N str), 1100, and 745 cm^{-1} (imide ring deformation).

Properties. The polyimides PI_p, PI_m, and PI_o obtained from the chemical imidization, were insoluble in organic solvents, such as NMP, DMSO, DMF, and DMAc. Although the chemical imidization of $PAEE_o$ proceeded homogeneously, the final polyimide PI_o (after

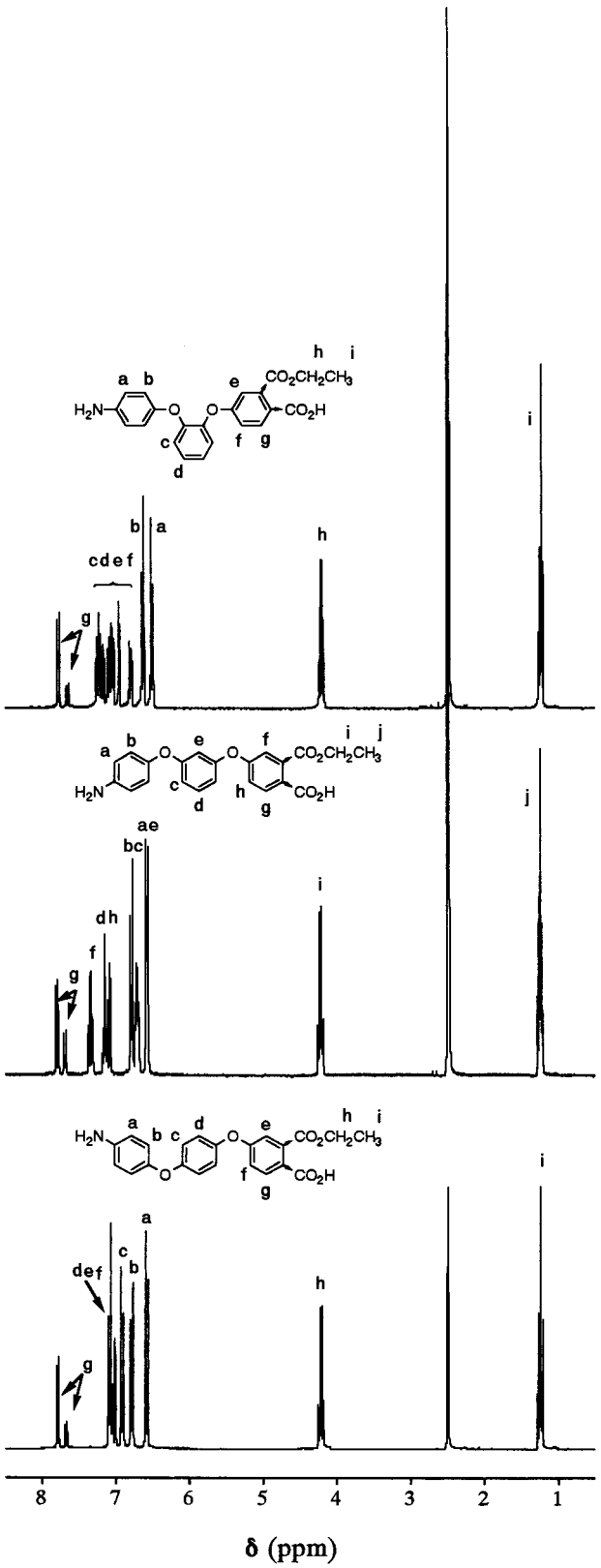

Figure 1. ^{1}H NMR spectra of AB-type monomers I_p, I_m, and I_o.

thermal treatment under vacuum at 250 °C for 24 h and at 300 °C for 1 h) could not be dissolved in organic solvents anymore. This might be attributed to the presence of crystalline structures in the final polyimides, as shown indirectly by the heat of melting of these polyimides (Table 3).

Table 1. Results of Direct Polycondensation of Isomeric Monomers I_p, I_m, and I_o[e]

polymer code	yield (%)	η_{inh}[a] (dL g)	M_w[b] (10^4)	M_n[b] (10^4)	PDI[b]	T_g[c] (°C)	T_i[d] (°C)
$PAEE_P$	93	0.31	8.00	3.52	2.3	159	203
$PAEE_m$	94	0.40	14.48	5.00	2.9	141	210
$PAEE_o$	90	0.31	8.46	4.14	2.0	147	215

[a] Measured in NMP at 30 °C (0.5 g/100 mL). [b] Obtained by GPC with polystyrene calibration. [c] Determined from the first DSC heating scan. [d] Obtained from the peak value of imidization in DSC first scan. [e] Polycondensation conditions: 1.20 g of monomer, 1.45 g of diphenyl (2,3-dihydro-2-thioxo-3-benzoxazolyl)phosphonate, 3.3 mL of NMP, at room temperature for 24 h.

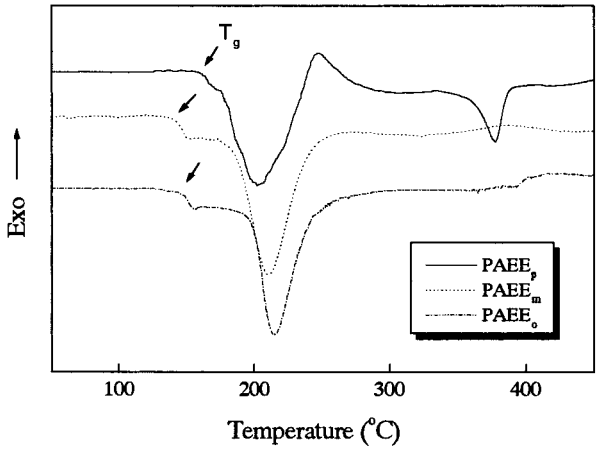

Figure 2. DSC thermograms of precursors $PAEE_p$, $PAEE_m$, and $PAEE_o$.

The crystallinities of the polyimide films PI_p, PI_m, and PI_o were evaluated by wide-angle X-ray diffraction measurements. The diffraction patterns, shown in Figure 3, indicate that all the three samples are semicrystalline polyimides. The crystallinity was estimated to be 24% for PI_p, 21% for PI_m, and 19% for PI_o, respectively. The main diffraction peaks were observed at 5.6, 17.5, and 18.4° for PI_p, 5.8, 17.3, and 18.9° for PI_m, and 7.1, 14.4, and 17.4° for PI_o.

The mechanical and thermal properties of the resulting polyimides were evaluated by tensile test, thermogravimetry (TG), differential scanning calorimetry (DSC), and dynamic mechanical analysis (DTA). The results are given in Table 2 (for polyimide films) and Table 3 (for polyimide powders). The tensile strength, elongation at break, and initial modulus of these polyimide films were in the range 98−231 MPa, 8−21%, and 1.9−2.3 GPa, respectively. Polyimide films PI_p and PI_m based on hydroquinone and resocinol were tough and flexible, and exhibited larger tensile strength (195−231 MPa) and elongation to break (15−21%) than those of PI_o. On the other hand, film PI_o was relatively brittle, and it cracked before reaching its glass transition temperature, as shown in Figure 4. These polyimides exhibited good thermal stability up to 500 °C, and they had almost the same temperature of 5% and 10% weight loss at about 555 and 570 °C, respectively. These results indicate that the difference in the structure of their repeating units did not affect their thermal decomposition temperature. Figure 5 shows the DSC thermograms of PI_p, PI_m, and PI_o. In the first heating scan (Figure 5A), all the polyimides showed a glass transition, and then displayed a single endotherm for PI_p and bimodal endotherm for PI_m and PI_o related to the melting transition. The samples were quenched to room temperature from

Table 2. Thermal and Mechanical Properties of AB-Type Polyimide Films

code	T_g[a] (°C)	T_s[b] (°C)	T_g[c] (°C) from E'/E''/tan δ	T_m[d] (°C)	ΔH_f[d] (J/g)	T_5/T_{10}[e] (°C)	char.[f] (%)	str[g] (MPa)	elong[h] (%)	modulus[i] (GPa)
PI_p	216	210	218/231/242	373.5	26.6	507/526	52	195	15	2.1
PI_m	176	175	189/193/202	333.7 337.4	16.8	558/570	55	231	21	2.3
PI_o	181	182	170/171/171	321.8 328.9 337.2	13.5	534/556	51	98	8	1.9

[a] From the second heating scan under nitrogen, heating rate, 5 °C/min. [b] Obtained by TMA measurement at a heating rate of 5 °C/min. [c] The glass transition temperature obtained from DMA measurement. [d] Melting transition temperature and enthalpy obtained from DSC first scan. [e] Temperature at which 5% (T_5) and 10% (T_{10}) weight loss recorded by thermogravimetry at a heating rate of 10 °C/min. [f] Residue weight % at 800 °C in nitrogen. [g] Load at break. [h] Elongation at break point. [i] Initial modulus.

Table 3. Thermal Properties of the Resulting AB-Type Polyimide Powders

code	T_m^1 (°C)[a]	ΔH_m^1 (J/g)[a]	T_m^2 (°C)[a]	ΔH_m^2 (J/g)[a]	T_g (°C)[b]	T_5 (°C)[c]	T_{10} (°C)[c]	char. (%)[d]
PI_p	393	31.1	391	29.3	198	556	571	55
PI_m	308 324	26.1	268[e] 313[e]	19.3[e]	178	560	572	59
PI_o	310 337	34.0			181	554	568	56

[a] Melting transition temperature and enthalpy obtained from DSC first scan (1a) and second scan (2a) at a heating rate of 5 °C/min. [b] From the second scan. [c] Temperature at which 5% (T_5) and 10% (T_{10}) weight loss recorded by thermogravimetry at a heating rate of 10 °C/min. [d] Residue weight % at 800 °C in nitrogen. [e] Obtained from the second scan of PI_m annealed at 250 °C for 24 h after melt treatment.

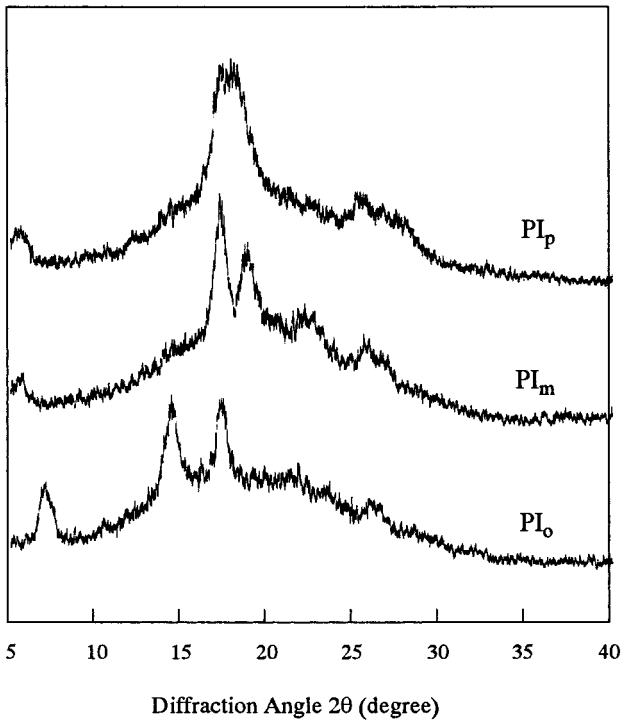

Figure 3. X-ray diffraction patterns of polyimide films PI_p, PI_m, and PI_o.

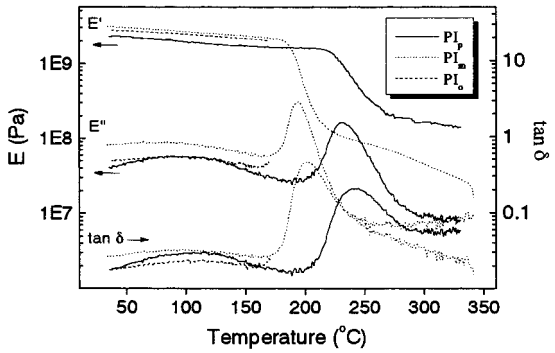

Figure 4. DMA curves of polyimide films PI_p, PI_m, and PI_o.

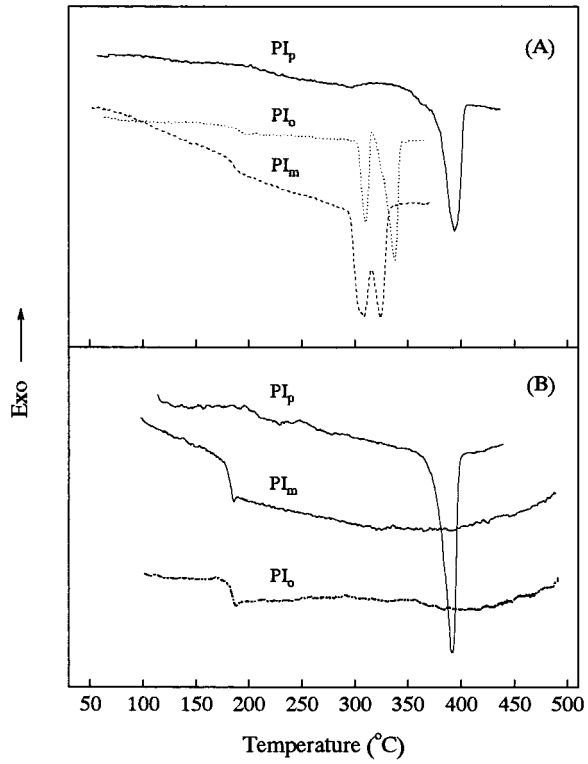

Figure 5. DSC thermograms of polyimides PI_p, PI_m, and PI_o: (A) first scan; (B) second scan.

the molten state followed by the second scan, as shown in Figure 5b. The glass transition temperatures were observed at 198 °C for PI_p, 178 °C for PI_m, and 181 °C for PI_o. The order of the glass transition temperature of these three polyimides was the same as that of their precursors, suggesting that polyimide with *m*-ether linkage was the most flexible. In the second scan of sample PI_p, a large endotherm associated with the melting transition of polyimide crystals was observed at 391 °C, close to the value (393 °C) obtained from the first scan. This must be indicative of fast crystallization of polyimide PI_p. The crystallization occurred during the quenching process from the molten state, and no exothermic peak was observed before the melting endotherm on the second scan. On the other hand, no obvious endotherm related to the melting transition was observed for sample PI_m and PI_o. This might be caused by the slow crystallization of these two polyimides. PI_m and PI_o were annealed by heating to 20 °C above their

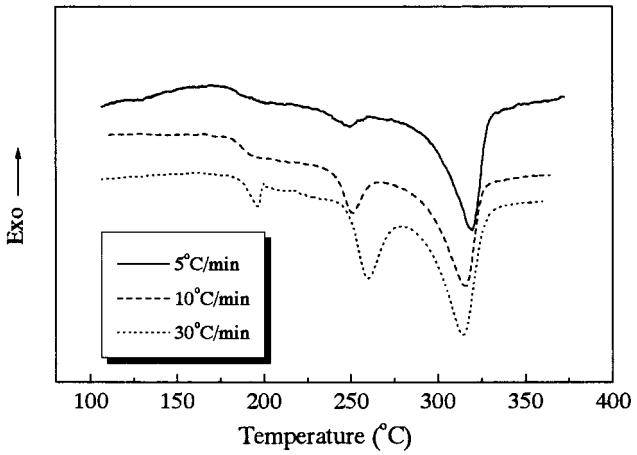

Figure 6. DSC thermograms of polyimide PI_m samples (isothermally crystallized at 226.8 °C for 1000 min) at different heating rates.

Table 4. Data of DSC Thermograms of PI_m Samples (Isothermally Crystallized at 226.8 °C for 1000 min) at Various Heating Rates

heating rate (°C/min)	T_m^1 (°C)[a]	heat of peak 1 (mJ/mg)	T_m^2 (°C)[b]	heat of peak 2 (mJ/mg)	heat of peak 2 to heat of peak 1
5	249.4	1.31	319.4	16.69	12.7
10	250.9	3.28	315.4	15.76	4.8
30	259.7	3.88	314.5	10.13	2.6

[a] The peak value of the first melting endotherm. [b] The peak value of the second melting endotherm.

respective melting transitions in the first scan, then cooled to 250 °C and kept for 24 h. The annealed PI_m displayed bimodal endotherm corresponding to the melting transition of the polymer crystals. On the other hand, the annealed PI_o did not exhibit any endotherm, similar to the second scan without annealing treatment. These results suggest that PI_m needs the annealing treatment to achieve crystalline structure once it was molten, and the crystallization of PI_o was extremely slow.

Melting Behavior. The multiple melting behavior has been reported in symmetric homopolyimides and copolyimides (prepared from AA/BB monomer systems),[8−9,11] as well as in poly(ether ether ketone).[19−22] They proposed several possibilities leading to the multiple melting behavior, such as (1) melting of the different crystal forms (polymorphisms); (2) melting associated with the melting/recrystallization process during heating; and (3) melting of the thinner and thicker lamellae.

To make sure if the cooling run at the end of the crystallization gave rise to any endotherms, one sample of PI_m was heated at the end of isothermal crystallization step without first cooling to room temperature. The melting behavior was essentially identical to the case when the sample was first cooled to room temperature prior to the second heating scan. This fact suggests that cooling to room temperature before the second heating scan does not result in any endotherm; the bimodal melting behavior is therefore caused by its isothermal crystallization and/or subsequent heating scan.

Figure 6 shows the DSC thermograms of polyimide PI_m (isothermally crystallized at 226.8 °C for 1000 min from the melt) under various heating rates. The results of the melting behavior are summarized in Table 4. It should be noted that, with an increase in the heating rate, (1) the first melting peak (peak 1) clearly shifted to a higher temperature, which is conventionally observed for the crystalline polymers, suggesting that the crystals associated with peak 1 exist in the isothermal crystallized sample, and (2) the second melting peak (peak 2) shifted to a lower temperature accompanied by the decrease in heat of melting. The higher the heating rate, the lower the heat ratio of peak 2 to peak 1. This result indicated that peak 2 is somewhat dependent on the heating rate, at least partially arisen from the melting of the crystals formed by melting/reorganization. At a slower heating rate, the crystals relevant to the first endotherm would experience greater residence time to convert to the crystals associated with the second endotherm via melting/reorganization process, and thus it would be expected to yield more "perfect" and thicker crystals. In contrast, at a faster heating rate, it would be expected to form less perfect and thinner crystals, leading to a relatively lower melting temperature.

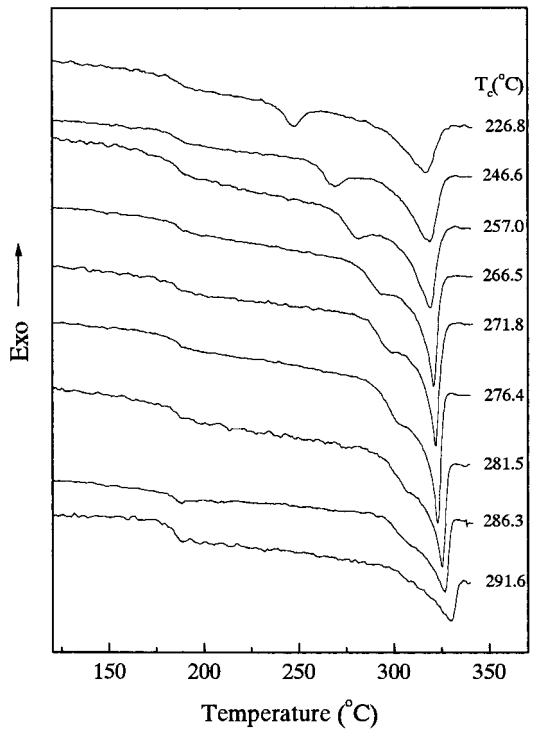

Figure 7. DSC thermograms of PI_m samples isothermally crystallized at various temperatures.

The effect of crystallization time on the melting behavior was also investigated by crystallizing PI_m samples at 226.8 °C for different length of times. The position and heat of the first melting peak gradually increased with the increase of crystallization time (peak value 243.9, 246.6, 247.4, and 249.3 °C and heat of melting 2.0, 2.9, 3.2, and 3.6 mJ/mg, respectively). On the other hand, the position and heat of the second melting peak were 319 °C and 17.0 mJ/mg, independent of crystallization time. These results suggested that the crystals relevant to peak 2 formed first, while those associated with peak 1 generated slowly.

Figure 7 shows the melting endotherms of PI_m samples isothermally crystallized at various temperatures after a melt treatment at 350 °C for 5 min. The first melting endotherm (peak 1) gradually shifted to higher temperature, and finally merged with the second endotherm. The values of peak 1 were observed at

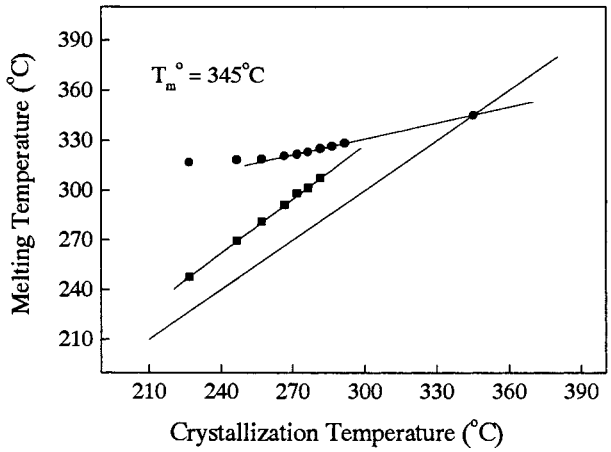

Figure 8. Hoffman−Weeks plot for polyimide PI_m.

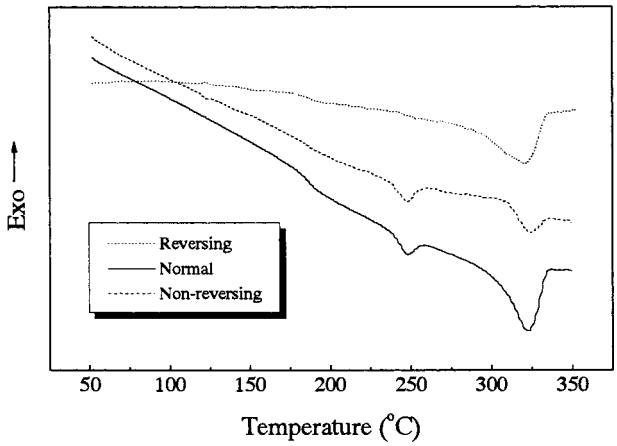

Figure 9. Temperature-modulated DSC thermograms of PI_m annealed at 226.8 °C for 48 h. (heating rate, 3 °C/min; amplitude, 0.4 °C; frequency,0.02 Hz; sample size, 5.00 mg).

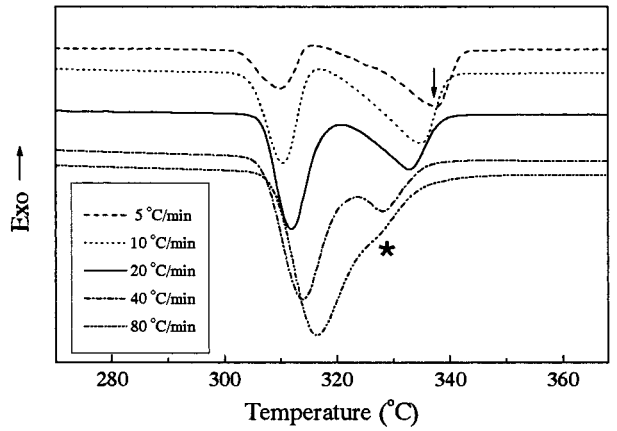

Figure 10. DSC thermograms for PI_o at various heating rates.

temperatures of ca. T_a + 20 °C, similar to the trends reported for the annealing (T_a + 10 °C) endotherm for other polymers.[23,24]

On the basis of the assignment of peak 2 to the melting of the primary crystals formed at the isothermal crystallization temperature (although it also probably contains the melting of the reorganized crystals), Hoffman−Weeks plot was constructed, as shown in Figure 8, to analyze multiple melting behavior and estimate the equilibrium melting temperature of this polyimide. The temperatures of peak 1 were parallel to the $T_m = T_a$ line, revealing that peak 1 did not arise from the primary crystals formed at the isothermal crystallization temperature. The points corresponding to peak 2 increased slightly with the increase of the annealing temperature, and the extrapolation of these points to the $T_m = T_a$ line gave an equilibrium melting temperature of 345 °C. Because of the overlap of the melting of primary crystals and reorganized crystals, the real value of the melting peak is somewhat different from that observed in DSC traces. Therefore, the value of the equilibrium melting temperature obtained here should be considered as a rough estimate of the real value.

Recently, a new thermal analytic technique TMDSC (temperature-modulated differential scanning calorimetry) has been used as an attractive approach to elucidate the melting and crystallization of polymers.[25] TMDSC measurement was carried out to identify if the second melting endotherm contains two kinds of melting kinetics. The total and reversing heat capacities (C_p^{total} and C_p^{rev}) were obtained using the Wunderlich method,[26] and the irreversing part was calculated by the equation $C_p^{irrev} = C_p^{total} - C_p^{rev}$, as shown in Figure 9. On the reversing curve, a glass transition and a broad melting endotherm were clearly observed. Two melting endotherms, at ca. 250 and 328 °C, came out on the irreversing curve. Although the explanation of TMDSC in detail is complicated, it is clear that the first melting endotherm belongs to the irreversible process, and the second melting endotherm in the total heat capacity curve (same as the normal DSC thermogram) contains two kinds of melting process, which could be attributed to the reversing and irreversing melting for preexisting crystals and reorganized crystals, respectively. It was reported that triple melting endotherms, corresponding to the melting of thinner crystals, thermally stable crystals, and reorganized crystals, were observed for AA/BB type polyimides. The melting behavior of PI_m should be essentially the same as those of AA/BB type polyimides, and the difference is the overlap of the melting of thermally stable crystals and reorganized crystals. Therefore, bimodal melting endotherms were observed in this work.

Another possibility for the multiple melting behaviors is associated with the melting of different crystal forms (polymorphisms). To clarify this possibility, we have prepared two semicrystalline samples of PI_m annealed at a lower (226.8 °C) and a higher (281.5 °C) temperature from the melt. These two PI_ms showed bimodal endotherms and one melting endotherm. Though the annealing at higher temperature produced relatively sharp and more defined peaks, the diffraction peak positions are found to be independent of annealing temperature. This suggests that the bimodal melting behavior is not caused by polymorphisms.

In the case of polyimide PI_o, the crystallization from the molten state was so slow that no endotherm could be observed on the subsequent heating scan even after annealing at 250 °C for 24 h. The as-made PI_o, therefore, was used to investigate the multiple-melting behavior. Figure 10 showed the DSC thermograms of PI_o at different heating rates. It could be observed that the first melting peak shifted gradually to higher temperature with the increase of heating rate. On the other hand, the second melting peak vanished rapidly. As expected, the melting of the primary crystals was observed (referred as asterisk) under higher heating rates. This phenomenon indicated that the second melting endotherm in Figure 5 probably included the

melting of the reorganized crystals as well. The multiple melting behavior of PI_o was most likely caused by the different crystal thickness and melting/reorganization process upon heating.

Conclusion

Three AB-type monomers (I_p, I_m, and I_o) based on hydroquinone, resorcinol and catechol, were synthesized in this paper. The polyimides were prepared via a two-step method, in which the direct polycondensation reactions carried out in NMP using DBOP as a condensing agent gave poly(amic acid ethyl ester)s followed by either chemical or thermal imidization to give the corresponding polyimides. The resultant polyimides were semicrystalline and exhibited good mechanical properties and thermal stability. The glass transition and melting transition temperatures were in the ranges 178−198 and 308−393 °C, respectively. The crystallinities of the AB-type polyimides PI_p, PI_m, and PI_o were estimated by means of X-ray diffraction measurements to be 19−24%. DSC studies revealed that polyimide PI_p based on hydroquinone crystallized much fast than those based on resorcinol and catechol. Polyimide PI_p showed a single melting endotherm, while PI_m and PI_o exhibited bimodal melting behavior. The bimodal melting behavior of PI_m and PI_o was probably associated with the different crystal thicknesses and the melting/recrystallization upon heating. The difference with the triple melting behavior of AA−BB polyimdes reported in the literature is the overlap of the melting of primary crystals and reorganized crystals.

Experimental Section

Materials. Commercially available hydroquinone, resocinol, catechol, 4-nitrophthalonitrile, 4-nitrofluorobenzene, and diphenyl(2,3-dihydro-2-thioxo-3-benzoxazolyl) phosphonate (DBOP) were purchased from Tokyo Kasei Organic Chemical Co. (TCI) and used without further purification. Extra pure methanol from Nacalai Tesque Inc. and DMF from Wako Pure Chemical Industries, Ltd. were used without purification. NMP were dried with calcium hydride overnight then distilled under reduced pressure. Acetic anhydride was dried with magnesium, followed by distillation under nitrogen before use. Other reagents were used as received.

Synthesis of 2_p, 2_m, and 2_o. As 5.50 g (0.05 mol) of hydroquinone was completely dissolved into 50 mL of dry methanol in 200 mL flask, which was dried by using heating gun under nitrogen, 2.70 g (0.05 mol) of sodium methoxide was added, and the mixture was stirred at room temperature for 1 h. After removal of methanol by evaporation, 50 mL of dry DMF and 6.90 g (0.04 mol) of 4-nitrophthalonitrile were added to the flask, followed by stirring at room temperature for 24 h. Then the mixture was poured into 1 L of cold and dilute hydrochloric acid. The crude product was collected by filtration, washed with water, and dried in a vacuum. Recrystallization from the mixture of ethanol and water using activated charcoal afforded 5.0 g of **2_p**, yield 53%. Mp: 150−151 °C. ^{1}H NMR (DMSO-d_6, ppm): δ 9.607 (s, 1H), 8.063−8.034 (d, 1H), 7.668−7.659 (d, 1H), 7.298−7.260 (q, 1H), 7.028−6.999 (m, 2H), 6.862−6.833 (m, 2H). IR (KBr): 3416, 2236, 1593, 1505, 1485, 1443, 1310, 1252, 1198, 1098, 1082, 949, 879, 833, 793 cm^{-1}. Anal. Calcd for $C_{14}H_8N_2O_2$ (236.22): C, 71.18; H, 3.41; N, 11.86. Found: C, 71.23; H, 3.32; N, 11.81.

From 5.50 g (0.05 mol) of catechol and 6.90 g (0.04 mol) of 4-nitrophthalonitrile, 5.19 g of **2_o** was obtained, yield 55%. Mp: 148−149 °C. ^{1}H NMR (DMSO-d_6, ppm): δ 9.906 (s, 1H), 8.042−8.013 (d, 1H), 7.631−7.623 (d, 1H), 7.203−7.114 (m, 3H), 7.036−7.004 (m, 1H), 6.917−6.861 (m, 1H). IR (KBr): 3348, 2247, 1603, 1586, 1511, 1485, 1366, 1297, 1254, 1224, 1185, 1098, 1083, 952, 870, 823, 787, 762 cm^{-1}. Anal. Calcd for $C_{14}H_8N_2O_2$ (236.22): C, 71.18; H, 3.41; N, 11.86. Found: C, 3.45; H, 71.40; N, 11.78.

A mixture of 8.0 g (0.073 mol) of resocinol, 8.9 g (0.051 mol) of 4-nitrophthalonitrile, 10 g (0.072 mol) of potassium carbonate, and 80 mL of DMF, was stirred at room temperature for 12 h. Then it was poured into cold dilute hydrochloric acid. The crude product was obtained by filtration, washed with water, and dried in a vacuum. After recrystallization from ethanol/water, 6.31 g of **2_m** was obtained, yield 52%. Mp: 161−162 °C. ^{1}H NMR (DMSO-d_6, ppm): δ 9.859 (s, 1H), 8.085−8.056 (d, 1H), 7.756−7.748 (d, 1H), 7.378−7.340 (q, 1H), 7.288−7.235 (t, 1H), 6.716−6.684 (q, 1H), 6.576−6.508 (m, 2H). IR (KBr): 3372, 2253, 1603, 1567, 1480, 1311, 1288, 1253, 1134, 975, 883, 800 cm^{-1}. Anal. Calcd for $C_{14}H_8N_2O_2$ (236.22): C, 71.18; H, 3.41; N, 11.86. Found: C, 71.33; H, 3.51; N, 11.79.

Synthesis of 3_p, 3_m, and 3_o. 5.0 g (0.021 mol) of **2_p**, 7.5 g of potassium hydroxide and 60 mL of H_2O were heated together at reflux for 24 h. After cooling to room temperature, the mixture was poured into 300 mL of cold, dilute hydrochloric acid. The crude product was collected by filtration, and dried in a vacuum. Recrystallization from the mixture of ethanol and water using activated charcoal afforded 5.3 g of **3_p**, yield 92%. Mp: 193−195 °C. ^{1}H NMR (DMSO-d_6, ppm): δ 9.438 (s, 1H), 8.177−8.148 (d, 1H), 7.593−7.583 (t, 1H), 7.034−6.925 (m, 3H), 6.822−6.794 (d, 2H). IR (KBr): 3230, 1728, 1690, 1603, 1576, 1508, 1425, 1300, 1223, 1196, 1064, 949, 835, 773 cm^{-1}. Anal. Calcd for $C_{14}H_{10}O_6$ (274.20): C, 61.33; H, 3.68. Found: C, 61.59; H, 3.74.

From 5.0 g (0.021 mol) of **2_m** (or **2_o**), after reaction and cooled to room temperature, the mixtures were neutralized with hydrochloric acid to pH 6−7, then extracted with ethyl acetate (3 × 60 mL). The extracts were dried with $MgSO_4$ overnight, then evaporated to remove ethyl acetate. The crude products, 5.1 g of **3_m**, 5.4 g of **3_o**, were obtained respectively after drying overnight at room temperature in a vacuum. These two products were used in next step without further purification.

Synthesis of 4_p, 4_m, and 4_o. A 5.80 g (0.021 mol) sample of **3_p**, 3.0 g (0.021 mol) of 4-nitrofluorobenzene, 15 g (0.1 mol) of CsF, and 60 mL of DMF were heated together at 100 °C for 24 h. After cooling to room temperature, the mixture was poured into 1 L of cold, dilute hydrochloric acid. The product was collected by filtration, washed with dilute hydrochloric acid, and dried in a vacuum. After recrystallization from aqueous acetic acid, 6.8 g of **4_p** was obtained, yield 81%. Mp: 218−220 °C. ^{1}H NMR (DMSO-d_6, ppm): δ 8.276−8.246 (m, 2H), 8.108−8.078 (d, 1H), 7.639−7.581 (m, 3H), 7.261−7.230 (m, 2H), 7.145−7.087 (m, 3H). IR (KBr): 3370, 1713, 1689, 1597, 1578, 1508, 1500, 1489, 1418, 1342, 1290, 1257, 1224, 1188, 1113, 1064, 846, 750 cm^{-1}. Anal. Calcd for $C_{20}H_{13}NO_8$ (395.28): C, 60.77; H, 3.31; N, 3.54. Found: C, 60.80; H, 3.46; N, 3.61.

From 5.1 g of **3_m** (or 5.4 g of **3_o**), the crude products, 6.0 g of **4_m** and 6.6 g of **4_o**, were obtained respectively, and they were used in the next step without further purification.

Synthesis of 5_p, 5_m, and 5_o. A mixture of 5.66 g (0.0143 mol) of **4_p**, 13 mL (0.13 mol) of acetic anhydride, and 20 mL of dry toluene were heated at reflux for 1 h, then the acetic anhydride and acetic acid were completely evaporated under reduced pressure. Recrystallization of the residue from toluene gave rise to 4.75 g of **5_p**, yield 88%. Mp: 162−163 °C. ^{1}H NMR (DMSO-d_6, ppm): δ 8.293−8.262 (q, 2H), 8.111−8.083 (d, 1H), 7.600−7.542 (m, 2H), 7.337 (s, 4H), 7.337−7.210 (m, 2H). IR (KBr): 3107, 1850, 1778, 1593, 1514, 1481, 1340, 1288, 1253, 1224, 1184, 1167, 1111, 1074, 893, 848, 738 cm^{-1}. Anal. Calcd for $C_{20}H_{11}NO_7$ (377.32): C, 63.66; H, 2.94; N, 3.71. Found: C, 64.21; H, 3.10; N, 3.73.

From 6.0 g of **4_m**, 4.9 g of **5_m** was obtained after recrystallization from toluene. Yield, 60% starting from **2_m**. ^{1}H NMR (DMSO-d_6, ppm): δ 8.276−8.246 (m, 2H), 8.108−8.078 (d, 1H), 7.639−7.581 (m, 3H), 7.261−7.230 (m, 2H), 7.145−7.087 (m, 3H). IR (KBr): 3077, 1848, 1777, 1585, 1510, 1478, 1351, 1261, 1225, 1119, 970, 895, 852, 730 cm^{-1}. Anal. Calcd for $C_{20}H_{11}NO_7$ (377.32): C, 63.66; H, 2.94; N, 3.71. Found: C, 64.16; H, 3.09; N, 3.74.

From 6.6 g of $\mathbf{4_o}$, 4.9 g of $\mathbf{5_o}$ (mp 154−155 °C) was obtained after recrystallization from toluene. Yield: 68% starting from $\mathbf{2_o}$. ^{1}H NMR (DMSO-d_6, ppm): δ 8.190−8.136 (m, 2H), 8.001−7.972 (d, 1H), 7.493−7.424 (m, 4H), 7.385−7.340 (m, 2H), 7.043−6.990 (m, 2H). IR (KBr): 3078, 1852, 1779, 1604, 1585, 1507, 1488, 1347, 1256, 1225, 1111, 1074, 906, 889, 737 cm^{-1}. Anal. Calcd for $C_{20}H_{11}NO_7$ (377.32): C, 63.66; H, 2.92; N, 3.71. Found: C, 64.34; H, 3.09; N, 3.75.

Synthesis of $\mathbf{6_p}$, $\mathbf{6_m}$, and $\mathbf{6_o}$. A mixture of 4.75 g (0.0126 mol) of $\mathbf{5_p}$ and 60 mL of pure ethanol was heated at reflux for 1 h. After cooling to room temperature, the resulting mixture was poured into 300 mL of ice−water. A 5.0 g yield of $\mathbf{6_p}$ was collected by filtration, washed with water, and dried in a vacuum at room temperature, yield 93%. ^{1}H NMR (DMSO-d_6, ppm): δ 8.282−8.251 (t, 2H), 7.865−7.728 (q, 1H), 7.315−7.169 (m, 8H), 4.287−4.216 (q, 2H), 1.301−1.240 (m, 3H). From the ^{1}H NMR spectrum, the isomeric ratio was determined to be *p*-/*m*-ethyl ester = 30:70 (molar ratio). IR (KBr): 3078, 2986, 1732, 1690, 1597, 1510, 1487, 1412, 1344, 1286, 1253, 1224, 1184, 1113, 1064, 1012, 949, 846, 750 cm^{-1}. Anal. Calcd for $C_{22}H_{17}NO_8$ (423.38): C, 62.41; H, 4.05; N, 3.31. Found: C, 62.71; H, 4.09; N, 3.26.

From 4.75 g (0.0126 mol) of $\mathbf{5_m}$, 5.1 g of $\mathbf{6_m}$ was obtained with a yield of 95%. ^{1}H NMR (DMSO-d_6, ppm): δ 8.273−8.230 (m, 2H), 7.842−7.701 (q, 1H), 7.575−7.521 (t, 1H), 7.252−7.182 (m, 4H), 7.068−7.002 (m, 3H), 4.267−4.196 (q, 2H), 1.279−1.217 (m, 3H). From ^{1}H NMR spectrum, the isomer ratio was determined to be *p*-/*m*-ethyl ester = 32:68 (molar ratio). IR (KBr): 3383, 3078, 1728, 1720, 1585, 1517, 1480, 1345, 1263, 1228, 1123, 1065, 973, 848, 750 cm^{-1}. Anal. Calcd for $C_{22}H_{17}NO_8$ (423.38): C, 62.41; H, 4.05; N, 3.31. Found: C, 62.64; H, 4.16; N, 3.30.

From 4.75 g (0.0126 mol) of $\mathbf{5_o}$, 5.1 g of $\mathbf{6_o}$ was obtained with a yield of 95%. ^{1}H NMR (DMSO-d_6, ppm): δ 8.187−8.144 (m, 2H), 7.751−7.608 (q, 1H), 7.440−7.357 (m, 4H), 7.046−6.911 (m, 4H), 4.239−4.156 (m, 2H), 1.260−1.193 (m, 3H). From the ^{1}H NMR spectrum, the isomeric ratio was determined to be *p*-/*m*-ethyl ester = 28:72(molar ratio). IR (KBr): 3075, 1739, 1606, 1609, 1576, 1513, 1490, 1343, 1288, 1252, 1214, 1112, 1066, 950, 850, 761, 750 cm^{-1}. Anal. Calcd for $C_{22}H_{17}NO_8$ (423.38): C, 62.41; H, 4.05; N, 3.31. Found: C, 62.59; H, 4.17; N, 3.29.

Synthesis of AB-Type Monomers: $\mathbf{I_p}$, $\mathbf{I_m}$, and $\mathbf{I_o}$. A mixture of 3.80 g (0.009 mol) of $\mathbf{6_p}$, 0.38 g of 10% palladium−charcoal catalyst, and 50 mL of dry ethanol (HPLC grade) was stirred vigorously under hydrogen at room temperature for 48 h. The reaction mixture was filtered with Celite to remove palladium−charcoal, and washed with 100 mL of ethanol. The filtrate was evaporated under reduced pressure. The product was dried in a vacuum at 35 °C for 5 days, giving rise to 3.4 g of I_p, yield 96%. ^{1}H NMR (DMSO-d_6, ppm): δ 7.808−7.663 (q, 1H), 7.106−7.004 (m, 4H), 6.944−6.890 (m, 2H), 6.806−6.760 (m, 2H), 6.612−6.560 (m, 2H), 4.251−4.180 (q, 2H), 1.271−1.208 (m, 3H). From the ^{1}H NMR spectrum, the isomeric ratio was determined to be *p*-/*m*-ethyl ester = 30:70 (molar ratio). IR (KBr): 3372, 2982, 1732, 1605, 1574, 1508, 1493, 1419, 1369, 1284, 1219, 1188, 1130, 1066, 1010, 837, 789 cm^{-1}. Anal. Calcd for $C_{22}H_{19}NO_6$ (393.40): C, 67.17; H, 4.87; N, 3.56. Found: C, 66.92; H, 5.15; N, 3.71.

From 3.8 g (0.009 mol) of $\mathbf{6_m}$, 3.42 g of I_m was obtained, yield 97%. ^{1}H NMR (DMSO-d_6, ppm): δ 7.817−7.681 (q, 1H), 7.377−7.322 (t, 1H), 7.176−7.081 (m, 2H), 6.807−6.691 (m, 4H), 6.608−6.568 (m, 3H), 4.260−4.189 (q, 2H), 1.278−1.216 (m, 3H). From ^{1}H NMR spectrum, the isomeric ratio was determined to be *p*-/*m*-ethyl ester = 32:68 (molar ratio). IR (KBr): 3371, 2981, 1719, 1594, 1508, 1479, 1369, 1268, 1209, 1125, 1066, 975, 837, 785 cm^{-1}. Anal. Calcd for $C_{22}H_{19}NO_6$ (393.40): C, 67.18; H, 4.83; N, 3.56. Found: C, 67.02; H, 5.13; N, 3.49.

From 3.8 g (0.009 mol) of $\mathbf{6_o}$, 3.4 g of I_o was obtained, yield 96%. ^{1}H NMR (DMSO-d_6, ppm): δ 7.804−7.656 (q, 1H), 7.276−6.966 (m, 5H), 6.836−6.796 (m, 1H), 6.659−6.620 (m, 2H), 6.534−6.505 (m, 2H), 4.251−4.204 (q, 2H), 1.270−1.210 (m, 3H). From ^{1}H NMR spectrum, the isomeric ratio was determined to be *p*-/*m*-ethyl ester = 28:72 (molar ratio). IR (KBr): 3373, 2981, 1720, 1607, 1576, 1508, 1490, 1369, 1265, 1211, 1106, 1066, 950, 883, 839, 773 cm^{-1}. Anal. Calcd for $C_{22}H_{19}NO_6$ (393.40): C, 67.17; H, 4.87; N, 3.56. Found: C, 66.90; H, 5.13; N, 3.54.

Direct Polycondensation. A 1.20 g (30.5 mmol) sample of the isomeric mixture I_p (or I_m, I_o), 1.46 g (37.1 mmol) of diphenyl(2,3-dihydro-2-thioxo-3-benzoxazolyl) phosphonate (DBOP), 0.43 mL of triethylamine (30.5 mmol), and 3.3 mL of *N*-methylpyrrolidone (NMP) were added to a three-neck flask, which was dried with a heating gun in a vacuum. The mixture was stirred at room temperature for 24 h under nitrogen and then diluted with NMP (12 mL) and poured into methanol (2 L) containing 0.01% lithium chloride. PAEE was collected and dried in a vacuum at 30 °C for 24 h.

Chemical Imidization. A mixture of 0.315 g of PAEE, 0.30 g of phthalic anhydride, 0.75 g of pyridine, and 6.0 mL of NMP was stirred at 100 °C for 24 h under nitrogen. After cooling to room temperature, the mixture was poured into 600 mL of methanol. The product was collected by filtration, washed with methanol, and dried in a vacuum at 250 °C overnight and at 300 °C for 1 h to ensure complete imidization.

Thermal Imidization of a Cast Film of PAEEs. A 0.5 g sample of PAEE was stirred with 2.0 mL of NMP overnight. Film cast onto the glass plate from the clear solution was put into a vacuum oven and heated 1 h each at room temperature, 100, 200, and 300 °C and then cooled to room-temperature slowly.

Measurements. Infrared (IR) spectra were recorded on a JASCO FTIR-8100 Fourier transform infrared spectrophotometer. ^{1}H and ^{13}C NMR spectra were recorded on a JEOL JNM-AL 300 MHz spectrometer. Thermogravimetric analysis (TGA) and differential thermal analyzer (DTA) were carried out with a Seiko TG/DTA 6200 at a heating rate of 10 °C/min under nitrogen. Differential scanning calorimetry (DSC) was performed on a Seiko DSC 6200 using a heating rate of 5 °C/min in nitrogen. Temperature-modulated differential scanning calorimetry (TMDSC) was carried out under the following measurement conditions: heating only; underlying heating rate, 3 °C/min; temperature amplitude, 0.4 °C; frequency, 0.02 Hz. Thermal mechanical analysis (TMA) was conducted on a Seiko TMA/SS6000 in penetration mode with a load of 10 g and a heating rate of 5 °C/min. Dynamic mechanical thermal analysis (DMA) was performed on a dynamic mechanical analyzer DVA-200S in tension mode at a heating rate of 5 °C/min and a frequency of 10 Hz. Inherent viscosity of poly(amic acid ethyl ester) was measured in NMP (0.5 g dL^{-1}) at 30 °C. Gel permeation chromatography (GPC) was performed on a JASCO HPLC 880PU fitted with polystyrene−divinylbenzene columns (two Shodex KD806 M and KD802) and a Shodex RI-71 refractive index detector in DMF containing 0.01 mol L^{-1} of lithium bromides as an eluent. Tensile tests were carried out on a TENSILON/UTM-II-20 machine with a strain rate 4 mm/min at room temperature, the specimens for the test are in the size of 40 × 5 mm, and the thickness of ca. 0.020 mm. Wide-angle X-ray diffraction patterns (WAXD) were recorded with a Rigaku RU-200 diffractometer using Ni-filtered Cu Kα radiation (50 KV, 180 mA, λ = 0.154 nm). The WAXD intensity is measured in the scattering angle range of 5−40° at a scanning speed of 1 °/min.

Acknowledgment. The authors thank Prof. Shigeo Asai, Prof. Toshiaki Ohgizawa and Dr. Susumu Umemoto of Tokyo Institute of Technology for X-ray diffraction and Temperature-Modulated DSC measurements, as well as further discussion on melting behavior of the aromatic polyimides.

References and Notes

(1) (a) Wilson, D.; Stenzenberger, H. D.; Hergenrother, P. M. *Polyimides* Blackie & Son Ltd.: Glasgow and London, 1990. (b) Ghosh, M. K.; Mittal, K. L. In *polyimides fundamentals and applications*; Marcel Dekker: New York, 1996.

(2) (a) Stenzenberger, H. D. *Adv. Polym. Sci*. **1994**, *117*, 165. (b) Takekoshi, T. *Adv. Polym. Sci.* **1999**, *140*, 1. (c) De Abajo, J.; De la Campa, J. G. *Adv. Polym. Sci.* **1999**, *140*, 23. (d)

Hedrick, J. L.; Carter, K. R.; Labadie, J. W.; Miller, R. D.; Volksen, W.; Hawker, C. J.; Yoon, D. Y.; Russell, T. P.; McGrath, J. E.; Briber, R. M. *Adv. Polym. Sci.* **1999**, *141*, 1. (e) Volksen, W. *Adv. Polym. Sci.* **1994**, *117*, 111.
(3) Heberer, D. P.; Cheng, S. Z. D.; Barlay, J. S.; Lien, S. H. S.; Bryant, R. G.; Harris, F. W. *Macromolecules* **1991**, *24*, 1890.
(4) Martin, D.; Berger, L. L.; Gardner, K. H. *Macromolecules* **1991**, *24*, 3921.
(5) Huo, P.; Cebe, P. *Polymer* **1993**, *34*, 696.
(6) Kim, Y. J.; Glass, T. E.; Lyle, G. D.; Mcgrath, J. E. *Macromolecules* **1993**, *26*, 1344.
(7) Eastmond, G. C.; Paprotny, J. *Macrololecures* **1995**, *28*, 2140.
(8) Kreuz, J. A.; Hsiao, B. S.; Renner, C. A.; Goff, D. L. *Macromolecules* **1995**, *28*, 6926.
(9) Hsiao, B. S.; Kreuz, J. A.; Cheng, S. Z. D. *Macromolecules* **1996**, *29*, 135.
(10) Eastmond, G. C.; Paprotny, J.; Irwin, R. S. *Macromolecules* **1996**, *29*, 1382.
(11) Srinivas, S.; Caputo, F. E.; Graham, M.; Gardner, S.; Davis, R. M.; McGrath, J. E.; Wilkes, G. L. *Macromolecules* **1997**, *30*, 1012.
(12) Ratta, V.; Stancik, E. J.; Ayambem, A.; Pavatareddy, H.; McGrath, J. E.; Wilkes, G. L. *Polymer* **1999**, *40*, 1889.
(13) Bell, V. L.; Stump, B. L.; Gager, H. *J. Polym. Sci.* **1976**, *14*, 2275.
(14) Hergenrother, P. M.; Havens, S. J. *J. Polym. Sci., Polym. Chem. Ed.* **1989**, *27*, 1161.
(15) Havens, S. J.; Hergenrother, P. M. *J. Polym. Sci., Part A: Polym. Chem.* **1987**, *25*, 2479.
(16) Hergenrother, P. M.; Wakelyn, N. T.; Havens, S. J. *J. Polym. Sci., Polym. Chem. Ed.* **1987**, *25*, 1093.
(17) Hergenrother, P. M.; Beltz, M. W.; Havens, S. J. *J. Polym. Sci., Part A: Polym. Chem.* **1991**, *29*, 1483.
(18) Liu, X. Q.; Yamanaka, K.; Jikei, M.; Kakimoto, M. *Chem. Mater.* **2000**, *12*, 3885.
(19) Blundell, D. J.; Osborn, B. N. *Polymer* **1983**, *24*, 953, 6937.
(20) Bassett, D. C.; Olley, R. H.; Al Raheil, I. A. M. *Polymer* **1988**, *29*, 1745.
(21) Lee, Y.; Porter, R. S.; Lin, J. S. *Macromolecules* **1989**, *22*, 1756.
(22) Lattimer, M P.; Hobbs, J. K.; Hill, M. J.; Barham, P. J. *Polymer* **1992**, *33* (18), 3971.
(23) Jonas, A. M.; Russell, T. P.; Yoon, D. Y. *Macromolecules* **1995**, *28*, 8491.
(24) Hsiao, B. S.; Sauer, B. B.; Verma, R. K.; Zachmann, H. G.; Seifert, S.; Chu, B.; Harney, P. *Macromolecules* **1995**, *28*, 6931.
(25) (a) Schawe, J. E. K.; Winter, W. *Thermochim. Acta* **1999**, *330*, 85. (b) Toda, A.; Tomita, C.; Hikosaka, M.; Saruyama, Y. *Polymer* **1998**, *39*, 5093. (c) Wunderlich, B.; Okazaki, I.; Ishikiriyama, K.; Boller, A. *Thermochim. Acta* **1998**, *324*, 77.
(26) Wunderlich, B.; Okazaki, I. *J. Thermal Anal.* **1997**, *49*, 57.

MA001862N